Low-Dimensional Manifolds in Reaction−Diffusion Equations. 2. Numerical Analysis and Method Development†

Michael J. Davis*

Chemistry Division, Argonne National Laboratory, Argonne, Illinois 60439

Received: September 30, 2005; In Final Form: December 19, 2005

Calculations are undertaken to study the approach to equilibrium for systems of reaction−diffusion equations on bounded domains. It is demonstrated that a number of systems approach equilibrium along attractive low-dimensional manifolds over significant ranges of parameter space. Numerical methods for generating the manifolds are adapted from methods that were developed for systems of ordinary differential equations. The truncation of the infinite spectrum of the partial differential equations makes it necessary to devise a new version of one of these methods, the well-known algorithm of Maas and Pope.

I. Introduction

A previous paper[1] demonstrated how low-dimensional manifolds arise in systems of reaction−diffusion equations. Most of the systems studied in ref 1 could be solved analytically as a sum over basis states. The purpose of the first paper was to explore fundamental aspects of these low-dimensional manifolds, so numerical complexity was downplayed. The present paper extends the analysis to systems whose solutions can only be obtained numerically and has two goals: (1) the demonstration that attractive low-dimensional manifolds are common over large regions of parameter space and (2) the development of methods for generating such manifolds.

The accurate modeling of reactive flows is computationally intensive,[2] and it is useful to have the means to gain computational savings. One way to do this is to develop methods for reducing the effort needed to model complex chemical kinetics, an important and time-consuming part of the modeling of reactive flows.[2] Chemical-kinetic systems often have a large range of time scales with the result that these systems approach equilibrium along low-dimensional surfaces (manifolds) in the phase space of the species. Because these manifolds have much lower dimension than the original system, they provide the potential for computational savings. Many researchers have studied these manifolds, with early reviews published elsewhere[3] and discussed in the first paper.[1] These manifolds are improvements to steady-state approximations[4] and are based on a better representation of the true dynamical nature of the kinetics. The work by Fraser and Roussel,[4−7] Lam and Goussis,[8] and Maas and Pope[9−11] are important examples of how dynamical information can be used to define low-dimensional manifolds in kinetics models. These works have motivated many others.[12−20] Reference 14 analyzes some of these methods in detail.

The methods outlined above rely on the reduction of the number of species that need to be followed to accurately model complex kinetics. That work naturally led to studies investigating the way transport processes important in the modeling of reactive flows could affect the reduction, and there have been several studies of this issue.[10,17,21,22] Reactive flows are solved in space and time,[2] and although it is important to understand the way that chemical-kinetic manifolds change due to transport processes, these manifolds are only one type of manifold that can be used to reduce the computational effort. Other types of low-dimensional manifolds provide greater computational savings, and these were studied in the first paper.[1] They go beyond the manifolds discussed in those earlier references in that they provide a reduction in both the number of species and the number of spatial points that need to be followed. They are qualitatively different than the ones discussed for systems of complex kinetics, as well as the modified versions of the manifolds studied in refs 10, 17, 21, and 22, and are related to inertial manifolds that have been studied for nonlinear partial differential equations.[23,24]

This paper continues the investigations of ref 1. It starts in section II by studying numerically a reversible association reaction with diffusion. This section investigates the conditions that lead to attractive one- and two-dimensional manifolds near equilibrium and then presents calculations demonstrating that these manifolds appear to exist well away from equilibrium. Section III then extends the analysis of section II, by adapting two methods for the study of low-dimensional manifolds for ordinary differential equations. The first is the algorithm of Maas and Pope,[9] and the second is the predictor−corrector method of ref 14. For systems of reaction−diffusion equations, no significant modification of the predictor−corrector method is necessary, but the Maas−Pope algorithm does require modifications. In addition, because the systems studied here are large, an effort is made to make the algorithm more efficient, and this is also described in section III. The methods described in section III are tested in section IV. The first test is for the nonlinear reaction−diffusion system of the first paper[1] that has an exact solution. Section IV also discusses the accuracy of the methods for the system of section II.

Sections V and VI extend the analysis to two systems studied previously by others. Section V studies the chain-branching system of ref 22 and section VI studies ozone combustion with the model of refs 17 and 25. These sections demonstrate that low-dimensional manifolds are common over a broad range of parameter space for chemically realistic systems. Section VII has a brief discussion and some conclusions.

† Part of the special issue "John C. Light Festschrift".

* Author to whom correspondence should be addressed. E-mail: davis@tcg.anl.gov.

10.1021/jp055593k CCC: $33.50
Published on Web 03/11/2006

II. Numerical Example: Reversible Association Reaction with Diffusion

A number of nonlinear systems have been studied numerically to investigate the finite-dimensional, attractive manifolds of ref 1, and results for three of these are presented here, along with a further investigation of the nonlinear system of section IV of the first paper.[1] The systems have the following form

$$\frac{\partial y_i}{\partial t} = G_i = F_i(\{y_j\}) + D_i \frac{\partial^2 y_i}{\partial x^2} \tag{2.1}$$

where the brackets refer to a set of species variables, for example, density, mass fraction, mole fraction, etc. The first term on the right refers to the reaction system, and the second term describes diffusion. All kinetics studied in this paper are isothermal.

This paper studies four systems, and there is a qualitative difference among them, characterized by the difference between the systems of refs 17 and 22. The system of ref 17 and section VI has a reaction component, F, which possesses a constant of motion

$$\sum m_i F_i = 0 \tag{2.2}$$

where the m_i values are integers. This is a common feature of reaction mechanisms,[2] where there can be several constants. The system of ref 22 and section V does not possess such a constant. Under conditions where there is a constant, the components in eq 2.1 can be summed

$$\frac{\partial w}{\partial t} = \sum_i m_i D_i \frac{\partial^2 y_i}{\sum x^2} \tag{2.3a}$$

with

$$w = \sum m_i y_i \tag{2.3b}$$

For systems where the D values are equal, eq 2.3a reduces to a diffusion equation

$$\frac{\partial w}{\partial t} = D \frac{\partial^2 w}{\partial x^2} \quad D_1 = D_i = D \tag{2.3c}$$

When D is small, eq 2.3c describes the slowest motion. For systems with small values of nearly equal D_i, the low-dimensional manifolds observed near equilibrium are analogous to the manifolds of eq 2.3c. There is no similar analogy for the manifolds of the other two systems studied here.

The model systems in this section and section IV[1] were studied in part because they correspond to the qualitative difference for the systems in section V and VI. The system studied in this section has a constant, and the system studied in section IV does not.

A. A System, Its Equilibrium States, and Their Stability. The reversible association reaction

$$\mathrm{A} \Leftrightarrow \mathrm{B} + \mathrm{B} \tag{2.4}$$

has the following reaction−diffusion system

$$\frac{\partial y_1}{\partial t} = -k_1 y_1 + k_2 y_2^2 + D_1 \frac{\partial^2 y_1}{\partial x^2} \tag{2.5a}$$

$$\frac{\partial y_2}{\partial t} = 2k_1 y_1 - 2k_2 y_2^2 + D_2 \frac{\partial^2 y_2}{\partial x^2} \tag{2.5b}$$

where k_1 and k_2 are the forward and reverse reaction rate constants, respectively, and y_1 and y_2 describe the densities or concentrations of A and B, respectively. In general, this system cannot be solved analytically. In this paper, boundary conditions are fixed in the same manner as in ref 1

$$y_1(x=0) = y_{10} \quad \frac{\partial y_1}{\partial x}(x=1) = 0 \tag{2.6a}$$

$$y_2(x=0) = y_{20} \quad \frac{\partial y_2}{\partial x}(x=1) = 0 \tag{2.6b}$$

The equilibrium state of the system in eq 2.2 is defined by

$$0 = -k_1 y_1^{\mathrm{eq}} + k_2 (y_2^{\mathrm{eq}})^2 + D_1 \frac{\partial^2 y_1^{\mathrm{eq}}}{\partial x^2} \tag{2.7a}$$

$$0 = 2k_1 y_1^{\mathrm{eq}} - 2k_2 (y_2^{\mathrm{eq}})^2 + D_2 \frac{\partial^2 y_2^{\mathrm{eq}}}{\partial x^2} \tag{2.7b}$$

In general, eq 2.7 must also be solved numerically. Two techniques are used to solve for the equilibrium states of the systems studied here. They are a Newton−Raphson procedure[26] and the "shooting" technique.[27] The latter technique is less stable and was only used in this section. The Newton−Raphson procedure was used for the cases in sections V and VI.

For $D_1 = D_2 = D$ in eq 2.5 the following is true

$$\frac{\partial w}{\partial t} = D \frac{\partial^2 w}{\partial x^2} \tag{2.8a}$$

with

$$w = 2y_1 + y_2 \tag{2.8b}$$

Near equilibrium the dynamics can be solved by linearization.[28] A displacement away from equilibrium in function space is described

$$\frac{\partial (y_1^{\mathrm{eq}} + \delta y_1)}{\partial t} = -k_1 (y_1^{\mathrm{eq}} + \delta y_1) + k_2 (y_2^{\mathrm{eq}} + \delta y_2)^2 + D_1 \frac{\partial^2 (y_1^{\mathrm{eq}} + \delta y_1)}{\partial x^2} \tag{2.9a}$$

$$\frac{\partial (y_2^{\mathrm{eq}} + \delta y_2)}{\partial t} = 2k_1 (y_1^{\mathrm{eq}} + \delta y_1) - 2k_2 (y_2^{\mathrm{eq}} + \delta y_2)^2 + D_2 \frac{\partial^2 (y_2^{\mathrm{eq}} + \delta y_2)}{\partial x^2} \tag{2.9b}$$

Because the displacements $\delta y_1$and δy_2 are small and y_1^{eq} and y_2^{eq} satisfy eqs 2.7a and 2.7b, the solution for the displacements is found from

$$\frac{\partial (\delta y_1)}{\partial t} = -k_1 \delta y_1 + 2k_2 (y_2^{\mathrm{eq}}) \delta y_2 + D_1 \frac{\partial^2 (\delta y_1)}{\partial x^2} \tag{2.10a}$$

$$\frac{\partial (\delta y_2)}{\partial t} = 2k_1 \delta y_1 - 4k_2 (y_2^{\mathrm{eq}}) \delta y_2 + D_2 \frac{\partial^2 (\delta y_2)}{\partial x^2} \tag{2.10b}$$

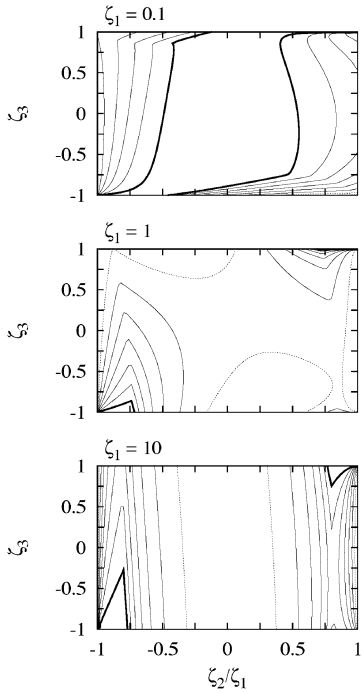

Figure 1. A series of contour plots of α_1 (eq 2.12) describing the local attraction to one-dimensional manifolds for a range of parameters. The parameters are defined in eq 2.11. The heading of each plot lists the value of ζ_1, the *x*-axes ζ_2/ζ_1, and *y*-axes ζ_3. The maximum contours in each plot are at 8.0 and are drawn as thick solid lines. The minimum contours in each plot are drawn as dotted lines and have the value of 4.0 in the top panel and 2.0 in the bottom two. The thin solid lines in the panels show the other contours that are at intervals of 1.0 between the minimum and the maximum contours.

Although eqs 2.10a and 2.10b are linear, the equilibrium distributions of the *y* values have a spatial dependence, and it is necessary to solve the equations numerically. Numerical solutions are accomplished with the discrete forms of eqs 2.10a and 2.10b, as outlined in ref 1. A grid of 99 internal points with a grid spacing of 0.01 was used for both y_1 and y_2.

Reference 1 described the stability analysis of systems such as the one in eq 2.5 starting from eq 2.10. The right-hand side of eq 2.10 defines a Jacobian matrix whose eigenvalues and eigenvectors define the dynamics locally. For such systems, the eigenvalue spectrum is infinite but is truncated, based on the number of grid points. Because of the truncation of the matrix only the lowest eigenvalues of the matrix are converged to any real degree.

The rest of the analysis of the equilibrium state and its stability follows from ref 1. A global analysis of the attractiveness of the linear manifolds near equilibrium is made in a similar manner as ref 1. The following parameters are defined

$$\zeta_1 = \frac{D_1 + D_2}{k_1 + k_2} \tag{2.11a}$$

$$\zeta_2 = \frac{D_1 - D_2}{k_1 + k_2} \quad -\zeta_1 \le \zeta_2 \le \zeta_1 \tag{2.11b}$$

$$\zeta_3 = \frac{k_1 - k_2}{k_1 + k_2} \quad -1 \le \zeta_3 \le 1 \tag{2.11c}$$

Figure 1 describes the attractiveness near equilibrium using the first two eigenvalues of the Jacobian matrix

$$\alpha_1 = \frac{\lambda_1}{\lambda_0} \tag{2.12}$$

Three sets of systems are studied in Figure 1 with different values of ζ_1. Contours are plotted between 2.0 and 8.0 with an interval of 1.0 for the bottom two panels and from 4.0 to 8.0 in the top panel. Most contours are plotted with solid lines, but the highest contours are drawn with a thicker solid line, and the lowest contours are drawn with dotted lines. As evident in Figure 1, there can be sharp corners in the contours because of seams in the surface that result from the presence of two different types of eigenvalues. Because there is no analytical form for the eigenvalues, as there was for most of the cases studied in ref 1, there has been no attempt here to generate these seams.

The top panel of Figure 1 demonstrates that when ζ_1 is small there is a wide range of parameter space near $D_1 = D_2$ where the manifolds are very attractive, and Figures 1b and 1c demonstrate that there is a more narrow range of parameters where attractiveness is large. There is a straightforward explanation for the regions of parameter space where attractiveness is high. In the top panel of Figure 1, diffusion is slow compared to reaction, and as long as the diffusion constants are not too different, the slow time scale is nearly purely diffusive (see above). In the bottom two panels diffusion competes with reaction, and a separation of time scales occurs for systems where the fast reacting species are those that also diffuse rapidly. Therefore the regions of parameter space where the attraction is highest are in the left bottom and right top of the middle and bottom panels of Figure 1. Both of these situations were studied in ref 1 for other systems, where it was possible to derive analytical values for the attractiveness globally.

Figure 2 shows the attractiveness of two-dimensional manifolds, defined as[1]

$$\alpha_2 = \frac{\lambda_2}{\lambda_1} \tag{2.13}$$

Equation 2.13 states that the attractiveness of the two-dimensional manifolds near equilibrium is estimated from the ratio of the second and third largest eigenvalues (both are negative). The top plot for $\zeta_1 = 0.1$ is very flat, and the only contour that appears is 2.0, which is plotted as a dotted line. (The maximum is 2.8.) The middle plot for $\zeta_1 = 1$ is less flat, and there are five contour values shown with the minimum at 2.0 plotted as a dotted line and the maximum contour of 6.0 in the bottom center plotted as a thicker solid line. The bottom panel of Figure 2 for $\zeta_1 = 10$ has a full range of contours from 2.0 to 8.0, as described above for the bottom two panels of Figure 1.

The contours in Figures 1 and 2 demonstrate that the system in eq 2.5 has attractive one-dimensional manifolds with attractiveness greater than 8.0 near equilibrium for a large range of parameter space for $\zeta_1 = 0.1$ and a much more limited range for $\zeta_1 = 1$ and $\zeta_1 = 10$. Two-dimensional manifolds near equilibrium are not very attractive over the whole range of parameter space for $\zeta_1 = 0.1$, but there are regions of parameter space where two-dimensional manifolds have high attractiveness for $\zeta_1 = 1$ and $\zeta_1 = 10$. In general, regions where two-dimensional manifolds are most attractive are those where the one-dimensional manifolds are least attractive and vice versa. This effect was previously observed in the first paper[1] for several systems.

B. Numerical Study of the Approach to Low-Dimensional Manifolds. It requires a numerical method to solve the time

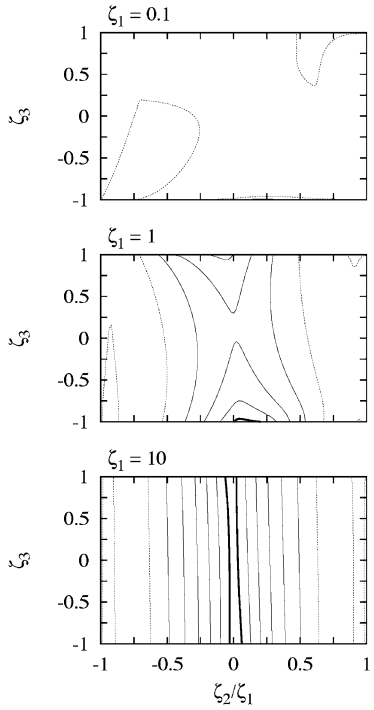

Figure 2. A series of contour plots describing the value of α_2 (eq 2.13) that describes the local attractiveness of two-dimensional manifolds. The values of the parameters are the same as in Figure 1, and the contour intervals are the same, but not all contours are present, because of the relative flatness of the top two panels. The dotted lines in the top panel show α_2 of 2.0, and the range of the contours in the middle panel is from 2.0 to 6.0, with the thicker curve in the bottom middle of the panel having that value.

development of the system, and a semidiscrete method is used.[29] The second derivatives in eq 2.5 are approximated with second-order finite differences, and the system of ordinary differential equations is solved with a stiff integrator, LSODE.[30]

Results for one of the systems pictured in each panel of Figure 1 are presented in the panels of Figure 3. These plots describe calculations on four initial distributions of y_1 and y_2. The top panel shows results for $(\zeta_1, \zeta_2, \zeta_3) = (0.1, 0.036, 0.7)$, the middle $(1, -0.82, -0.92)$, and the bottom $(10, -8.6, -0.56)$. The x-axes of the top two panels describe the value of y_1 at $x = 0.59$ and the y-axes indicate the value of y_2 at $x = 0.18$. The bottom plot shows results for y_1 at $x = 0.19$ and y_2 at $x = 0.91$. The large dots on all the panels show the value of the equilibrium distributions at the selected coordinate pairs. The plots in Figure 3 show that the near-equilibrium attraction indicated in Figure 1 extends away from equilibrium, and the bottom two panels indicate that the manifolds are nearly linear in those cases. The plots in Figure 3 demonstrate that the time propagation of the four initial distributions in each panel approach one-dimensional manifolds.

The analysis of Figure 3 is extended in Figure 4 to a case from Figure 2 for a two-dimensional manifold. Four distributions are studied. The parameter values for this case are $(\zeta_1, \zeta_2, \zeta_3) = (1, 0.04, -0.98)$. As indicated in the middle panel of Figure 1, this case has one-dimensional manifolds with very low attractiveness, and the top panel of Figure 4 demonstrates this with the propagation of four initial distributions. The projection used in this case is $y_1(x = 0.30)/y_2$ $(x = 0.47)$, and the large dot is the projection of the equilibrium distribution. The plot demonstrates that the distributions do not approach a one-dimensional manifold with any real degree of attraction.

Although one-dimensional manifolds are not very attractive for this set of parameters, two-dimensional manifolds are. The

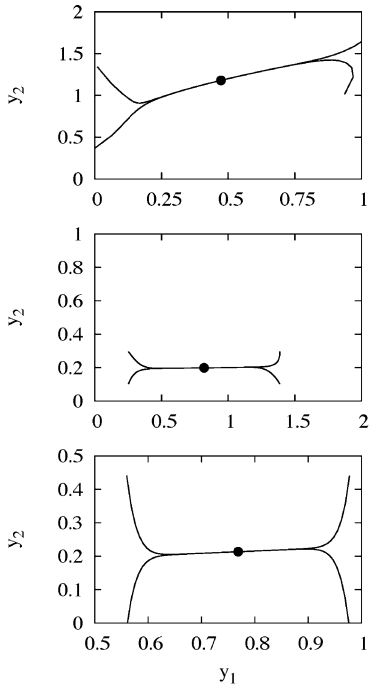

Figure 3. Results for a set of distributions plotted here using $y_1(x_\beta)/y_2(x_\sigma)$ projections. The systems studied in the panels correspond to one system from each of the panels of Figures 1 and 2, with the full list of parameters noted in the text. In the top two panels $x_\beta = 0.59$ and $x_\sigma = 0.18$. In the bottom panel $x_\beta = 0.19$ and $x_\sigma = 0.91$.

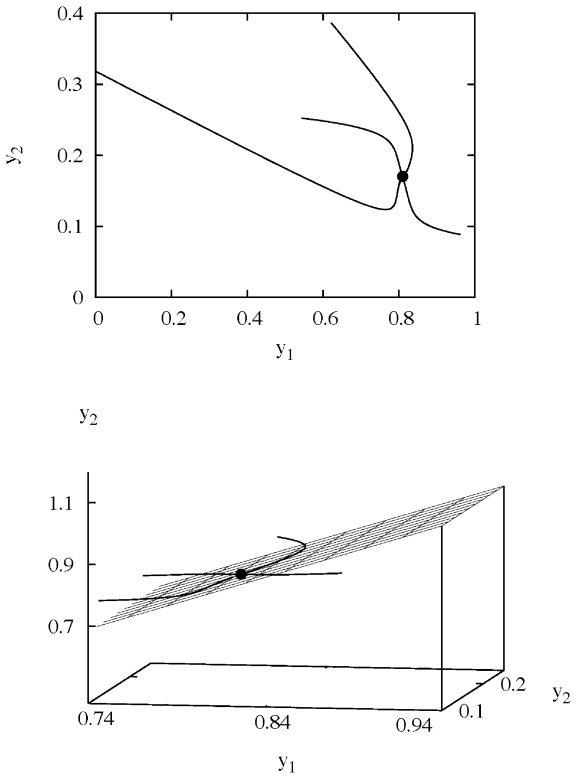

Figure 4. Results from a set of four calculations plotted in these two panels for $(\zeta_1, \zeta_2, \zeta_3) = (1, 0.04, -0.98)$. The top panel shows a two-dimensional projection for $y_1(x_\beta)/y_2(x_\sigma)$, and the bottom a three-dimensional projection for $y_1(x_\beta)/y_2(x_\sigma)/y_1(x_\phi)$. The values of the spatial coordinates are: $x_\beta = 0.30$, $x_\sigma = 0.47$, and $x_\phi = 0.60$. The plane plotted in the bottom panel is formed from the first two eigenvectors whose eigenvalues are λ_0 and λ_1.

value of α_2 indicated in the middle plot of Figure 2 is 6.1. The bottom panel of Figure 4 shows a three-dimensional projection

of the same set of results from the top plot (y_1 ($x = 0.3$)/y_2 ($x = 0.47$)/y_1 ($x = 0.6$)). Also included in the bottom panel of Figure 4 is the plane defined by the two eigenvectors of the Jacobian whose eigenvalues define α_1 (eq 2.12) for the one-dimensional manifolds. These eigenvectors are the ones whose eigenvalues have the two least negative real parts. The bottom plot indicates that, while the trajectories in the top panel do not approach a one-dimensional manifold, they do approach a plane, indicative of a two-dimensional manifold.

The results in this section and ref 1 demonstrate that there are systems whose time development approaches low-dimensional manifolds on the way to equilibrium. The rest of the paper will extend these earlier numerical and analytical studies. Two methods of approximating low-dimensional manifolds away from equilibrium will be developed, and their accuracy will be investigated. These methods are general enough that they can be applied to more complex cases than those investigated here.

III. A New Version of the Maas−Pope Algorithm

The low-dimensional manifolds studied here are difficult to estimate with many of the techniques discussed in the Introduction, because of the large dimensionality of the system of ordinary differential equations used to approximate the reaction−diffusion systems, and only two techniques are used. One is the predictor−corrector method of ref 14, and the other is the Maas−Pope algorithm of refs 9−11. There have been no significant modifications of the predictor−corrector method, and the description in ref 14 is sufficient. Significant modifications have been made to the Maas−Pope algorithm, and they are now described.

One of the most complete descriptions of the numerical issues involved in applying the Maas−Pope algorithm is presented in ref 11. As this reference makes clear, there are a number of important problems that arise in trying to implement the algorithm. Two of these problems become particularly acute when studying the systems in this paper.

Consider the Jacobian matrix **J**, for the semidiscrete form of the reaction−diffusion system for the association reaction of section II. It is written in a block form[1]

$$\mathbf{J} = \begin{pmatrix} J^{11} & J^{12} \\ J^{21} & J^{22} \end{pmatrix} \tag{3.1}$$

and has the following matrix elements

$$J^{11}_{kk} = -k_1 - \frac{2D_1}{\Delta x^2} \quad J^{11}_{k,k+1} = J^{11}_{k,k-1} = \frac{D_1}{\Delta x^2}$$
$$J^{11}_{km} = 0 \text{ for all other } m \text{ values} \tag{3.2a}$$

$$J^{21}_{kk} = 2k_1 \quad J^{21}_{\mathrm{km}} = 0 \text{ for all other } m \text{ values} \tag{3.2b}$$

$$J^{12}_{kk} = 2k_2 y_{2k} \quad J^{12}_{km} = 0 \text{ for all other } m \text{ values} \tag{3.2c}$$

$$J^{22}_{kk} = -4k_2 y_{2k} - \frac{2D_2}{\Delta x^2} \quad J^{11}_{k,k+1} = J^{11}_{k,k-1} = \frac{D_2}{\Delta x^2}$$
$$J^{11}_{km} = 0 \text{ for all other } m \text{ values} \tag{3.2d}$$

Because the Jacobian is a real general matrix, it possesses left and right eigenvectors that are defined by the following matrix equation[31]

$$\mathbf{L}^{\mathrm{T}}\mathbf{J}\mathbf{R} = \Lambda \tag{3.3}$$

where **L** and **R** refer to left and right eigenvectors and the superscript "T" refers to the transpose of matrix **L**. The eigenvalues of **J** are contained in the diagonal matrix Λ.

The first of the problems noted above arises because the eigenvalues and eigenvectors of **J** are generated from a truncated version of **J**, and the higher eigenvalues and their respective eigenvectors are generally not converged, making them very sensitive to small changes in the elements of **J**. This makes many algorithms for implementing the Maas−Pope approximation unstable. The second problem is due to the large number of ordinary differential equations defined by a semidiscrete method. For only a few species and grids of a hundred points per species, the system of ordinary differential equations contains on the order of a few hundred equations and makes the Newton−Raphson searches to satisfy the manifold conditions[11] long.

These two problems have led to the development of an alternate algorithm that only uses the relevant eigenvector space, the "slow space".[11] The new algorithm is now described for one- and two-dimensional manifolds. Extension to higher-dimensional manifolds is straightforward. All manifolds studied in this paper are one-dimensional and two-dimensional, because they are the most attractive for the systems studied.

The Maas−Pope approximation starts with the assumption that a system rapidly relaxes to a lower-dimensional manifold defined locally by a subspace spanned by the slow eigenvectors of the Jacobian. These eigenvectors are the right eigenvectors whose eigenvalues are those with negative real parts and the lowest in magnitude. An m-dimensional manifold in an n-dimensional space ($m < n$) is defined locally by m eigenvectors with this condition on the eigenvalues. In many versions of the algorithm, the condition is implemented by making sure that the space of "fast" eigenvectors lies perpendicular to the manifold. The fast eigenvectors are the other eigenvectors that are not "slow", that is those whose eigenvalues have a larger magnitude. Because **J** is a real general matrix, both the left and the right eigenvectors need to be used to satisfy this condition.[9] For the systems studied here, such an algorithm is not stable, because many of the fast eigenvalues are not converged (problem 1), and a new algorithm is needed and is now developed.

Consider a system of ordinary differential equations, which in this paper is a spatially discrete approximation of a system of partial differential equations. The time development of the kth coordinate of this n-dimensional system is

$$\frac{\mathrm{d}y_k}{\mathrm{d}t} = F_k(\{y_j\}) \quad j = 1 \rightarrow n \tag{3.4}$$

An element of the Jacobian matrix is defined as

$$J_{km} = \frac{\partial F_k}{\partial y_m} \tag{3.5}$$

The right and left eigenvectors of **J** satisfy eq 3.3 and are orthogonal to each other in the following manner

$$\mathbf{L}^{\mathrm{T}}\mathbf{R} = \mathbf{I} \tag{3.6}$$

where **I** is the identity matrix. The elements of **R** are written as

$$R_{km} \tag{3.7}$$

The elements of the right eigenvector whose eigenvalue is negative and smallest in magnitude is labeled as "1", and its elements are written as

$$R_{k1} \tag{3.8}$$

The new version of the Maas−Pope algorithm is implemented by finding the set of y values in eq 3.4 whose "velocity" vector (the right-hand side of eq 3.4) lines up along the slow eigenspace of the right eigenvectors. The implementation of this procedure is now described for a one-dimensional manifold. The most straightforward way to implement the condition is to choose one of the coordinates locally as the "independent" coordinate and all of the other $n - 1$ coordinates as "dependent". The Maas−Pope condition is then written

$$\frac{R_{k1}}{R_{m1}} = \frac{F_k}{F_m} \quad k = 1 \rightarrow \mathrm{n} \quad k \neq m \tag{3.9}$$

where y_m is chosen as the independent variable and the rest of the variables are the dependent variables.

To solve the set of $n - 1$ conditions described in eq 3.9, they are rewritten as the following set of $n - 1$ functions

$$S_k \equiv R_{m1}F_k(x) - R_{k1}F_m(x) \quad k = 1 \rightarrow n \quad k \neq m \tag{3.10}$$

The following set of $n - 1$ conditions then define the Maas−Pope approximation to the one-dimensional manifold

$$S_k = 0 \quad k = 1 \rightarrow n \quad k \neq m \tag{3.11}$$

Equation 3.11 is an $(n - 1)$-dimensional system that is solved by first fixing y_m and then making a search for the rest of the y_k values. From experience,[11] it is important to have a good first guess to eq 3.11 at a given value of y_m to find an accurate approximation to the manifold. Good guesses are obtained by starting near equilibrium and carefully moving away from it, with convergence attained at a set of points along the manifold.[14] However, even with careful first guesses, searches can be time-consuming. For example, in searches using the Newton−Raphson procedure[32] (which is what is used here), it is necessary to find the derivatives of the right-hand side of eq 3.4 in terms of the $(n - 1)$-dependent coordinates. The most straightforward way to do this is with finite-difference approximations to the derivatives. However, this procedure requires the diagonalization of $n - 1$ $n \times n$ matrices and is very time-consuming.

A more efficient search is now developed. Equation 3.11 is solved by a Newton−Raphson method, and this requires a Jacobian matrix for S in eq 3.11, denoted $\mathbf{J}^S$ to distinguish it from other Jacobian matrices in this paper. The kj element of this Jacobian matrix is

$$J^S_{kj} = \frac{\partial S_k}{\partial y_j} = R_{m1}\frac{\partial F_k}{\partial y_j} + F_k\frac{\partial R_{m1}}{\partial y_j} + R_{k1}\frac{\partial F_m}{\partial y_j} + F_m\frac{\partial R_{k1}}{\partial y_j} \tag{3.12}$$

which is derived by chain-rule differentiation of eq 3.10. The first and third terms on the right-hand side of eq 3.12 are already known from the original Jacobian matrix of the F values and the eigenvectors of that Jacobian. The second and fourth terms lead to increased computational cost. If finite differences are used to calculate the R derivatives, $(n - 1)$ $n \times n$ matrix diagonalizations must be performed. To reduce this effort, an "analytical" method is used to solve for the eigenvector derivatives.[33] This method uses both left and right eigenvectors but only needs a single right eigenvector and its corresponding left eigenvector to define the derivative of that particular right eigenvector. So when eq 3.11 is solved, only the first right and left eigenvectors are needed in the search based on eq 3.12. The method requires matrix-vector operations, and second derivatives are needed. Both of these have some computational cost, but this cost is low enough that there is typically a factor of 50 savings for a case with $n = 100$.

A two-dimensional manifold is defined by fixing two of the coordinates as "independent", labeled here as y_m and y_p. There are $n - 2$ conditions that define the Maas−Pope approximation for a two-dimensional manifold, and these are analogous to eqs 3.10 and 3.11 for one-dimensional manifolds. The conditions are

$$Q_{mp}F_k - Q_{kp}F_m + Q_{km}F_p = 0 \tag{3.13a}$$

with

$$Q_{mp} = R_{m1}R_{p2} - R_{p1}R_{m2} \tag{3.13b}$$

$$Q_{km} = R_{k1}R_{m2} - R_{k2}R_{m1} \tag{3.13c}$$

$$Q_{kp} = R_{k1}R_{p2} - R_{k2}R_{p1} \tag{3.13d}$$

where R_{k2}, R_{m2}, and R_{p2} refer to the elements of the second right eigenvector, which is the eigenvector whose eigenvalue is the next "least negative". R_{k1}, R_{m1}, and R_{p1} are elements of the previously discussed first right eigenvector. The search for the $(n - 2)$-dependent y values is similar to what was described for the $n - 1$ conditions used to find a one-dimensional manifold described above.

IV. Tests of Manifold Methods

A. Exact Maas−Pope Results Compared to Exact Manifolds. The methods derived in the previous section are now tested. This is done first for the system of section IV of ref 1

$$\frac{\partial y_1}{\partial t} = -y_1 + D_1\frac{\partial^2 y_1}{\partial x^2} \tag{4.1a}$$

$$\frac{\partial y_2}{\partial t} = -\gamma y_2 + a{y_1}^2 + D_2\frac{\partial^2 y_2}{\partial x^2} \tag{4.1b}$$

The boundary conditions are the same as those in ref 1 (see eq 2.6 above). The calculations in ref 1 focused on the case $a = \gamma - 2$, because the pure kinetics part of the problem ($D_1 = D_2 = 0$) has a simple one-dimensional manifold: $y_2 = {y_1}^2$. Earlier work on the Maas−Pope algorithm[14,34] has made it clear that there are two components to the error, the curvature and the attractiveness, studied in section II for the association reaction. The attractiveness of manifolds was one of the main focuses of ref 1, and it does not depend on a.[1] However the curvature does depend on a, and to make a complete test of the Maas−Pope algorithm it is necessary to investigate a range of values of a other than $\gamma - 2$.

Appendix A derives the Maas−Pope approximation to the manifolds studied previously in ref 1. As ref 1 discussed, there are two types of one-dimensional manifolds, depending on the parameters of the system, and these were labeled case 1 and case 2 (eq 4.6 in ref 1). These cases give rise to four types of two-dimensional manifolds labeled 1_1, 1_2, 2_1, and 2_2. One-dimensional manifolds of type 1 and two-dimensional manifolds of type 1_1 and 1_2 are studied in this section.

The Maas−Pope approximation for one-dimensional manifolds of type 1 is written in the standard form of ref 1

$$y_{1\sigma} = \frac{\sin\left(\frac{\pi x_\sigma}{2}\right)}{\sin\left(\frac{\pi x_\beta}{2}\right)} y_{1\beta} \tag{4,2a}$$

$$y_{2\phi} = \tau_{20}^{\mathrm{MP}}(x_\phi) \frac{y_{1\beta}^2}{\left(\sin\frac{\pi x_\beta}{2}\right)^2} + \tau_{30}^{\mathrm{MP}}(x_\phi) \frac{y_{1\beta}}{\sin\frac{\pi x_\beta}{2}} \tag{4.2b}$$

where x_β, x_σ, and x_ϕ refer to specific values of the spatial coordinate x.[1] The spatial domain is fixed to be the unit interval, so the x values lie between 0 and 1. The following definitions are used for the species coordinates in eqs 4.2a and 4.2b[1]

$$y_{1\beta} \equiv y_1(x_\beta) - y_1^{\mathrm{eq}}(x_\beta) \tag{4.3a}$$

$$y_{1\sigma} \equiv y_1(x_\sigma) - y_1^{\mathrm{eq}}(x_\sigma) \tag{4.3b}$$

$$y_{2\phi} \equiv y_2(x_\phi) - y_2^{\mathrm{eq}}(x_\phi) \tag{4.3c}$$

The designation "eq" refers to equilibrium distributions of the species. Equations 4.2a and 4.2b indicate that the form of the type 1 manifolds in the Maas−Pope approximation is the same as the exact manifold. The differences are in the functions τ_{20} and τ_{30}, which are labeled here with the superscript "MP", indicating the Maas−Pope approximation.

As expected,[34] the Maas−Pope algorithm gives the exact answer for the function in front of the linear term

$$\tau_{30}^{\mathrm{MP}} = \tau_{30} \tag{4.4}$$

The Maas−Pope estimate for the function in front of the quadratic term, τ_{20}, differs from the exact version. The function τ_{20} is written as a sum over basis states

$$\tau_{20}(x) = \sum_{\mathrm{m}} \mathrm{T}_m \sin\left[\left(m + \frac{1}{2}\right)\pi x\right] \tag{4.5a}$$

and the Maas−Pope and exact versions can be compared

$$\mathrm{T}_m^{\mathrm{MP}} = \frac{a\left[(\gamma+1) + \left(m+\frac{1}{2}\right)^2\pi^2 D_2 + \frac{\pi^2 D_1}{4}\right] r_{00}^m}{\left[\gamma + \left(m+\frac{1}{2}\right)^2\pi^2 D_2\right]\left[(\gamma-1) + \left(m+\frac{1}{2}\right)^2\pi^2 D_2 - \frac{\pi^2 D_1}{4}\right]} \tag{4.5b}$$

$$\mathrm{T}_m = \frac{a r_{00}^m}{(\gamma-2) + \left(m+\frac{1}{2}\right)^2\pi^2 D_2 - \frac{\pi^2 D_1}{2}} \tag{4.5c}$$

where the "MP" once again refers to the Maas−Pope approximation and eq 4.5c shows the exact result.

The absolute error for the Maas−Pope approximation is

$$\mathrm{T}_m - \mathrm{T}_m^{\mathrm{MP}} \equiv -E_{20} = \frac{-2a[\lambda_0^{(1)}]^2 r_{00}^m}{\lambda_m^{(2)}[\lambda_m^{(2)} - \lambda_0^{(1)}][\lambda_m^{(2)} - 2\lambda_0^{(1)}]} \tag{4.6a}$$

$$E_{20} = \frac{2a\delta_m^2 r_{00}^{\mathrm{m}}}{\lambda_m^{(2)}[1-\delta_m][1-2\delta_m]} \tag{4.6b}$$

where

$$\lambda_k^{(1)} = -\left[1 + \pi^2\left(k+\frac{1}{2}\right)^2 D_1\right] \tag{4.7a}$$

$$\lambda_k^{(2)} = -\left[\gamma + \pi^2\left(k+\frac{1}{2}\right)^2 D_2\right] \tag{4.7b}$$

$$\delta_m \equiv \frac{\lambda_0^{(1)}}{\lambda_m^{(2)}} \tag{4.7c}$$

and r_{00}^m is an integral defined in eq A.3a. The relative error is

$$E_{20}^{(r)} = \frac{\mathrm{T}_m - \mathrm{T}_m^{\mathrm{MP}}}{\mathrm{T}_m} = \frac{2(\delta_m)^2}{(1-\delta_m)} \tag{4.8}$$

Equations 4.6−4.8 indicate that the absolute error is first-order in the curvature (the parameter a) and second-order in the eigenvalue ratio defined in eq 4.7c. The relative error of eq 4.8 does not depend on curvature at all and is second-order in δ for small values of δ. The errors indicated in these equations are somewhat different than those calculated for systems of ordinary differential equations,[14,34] because they do not depend directly on the attractiveness of the one-dimensional manifolds. The attractiveness depends on the ratio $\lambda_1^{(1)}/\lambda_0^{(1)}$ rather than δ_m in eq 4.7c. It is also different, because the relative error does not depend on the curvature at all.

The two-dimensional manifolds of type 1_1 were defined in ref 1. They depend on the functions τ_{20}, τ_{21}, τ_{22}, τ_{30}, and τ_{31}, which are written as expansions. The functions τ_{20} and τ_{30} have already been defined for one-dimensional manifolds, and the error in the Maas−Pope estimate is the same. The Maas−Pope estimate for the τ_{31} term, like the τ_{30}, is exact. The other two functions have the following relative error for each term in the expansion

$$E_{21}^{(r)} = \frac{\epsilon_m\delta_m[2-\epsilon_m-\delta_m]}{(1-\epsilon_m)(1-\delta_m)} \tag{4.9a}$$

$$E_{22}^{(r)} = \frac{2(\epsilon_m)^2}{(1-\epsilon_m)} \tag{4.9b}$$

with δ defined in eq 4.7c and

$$\epsilon_m \equiv \frac{\lambda_1^{(1)}}{\lambda_m^{(2)}} \tag{4.10}$$

Once again errors depend on the ratio of eigenvalues and do not depend on curvature.

The absolute and relative errors in the Maas−Pope approximation for one-dimensional manifolds of type 1 depend on δ_m, defined in eq 4.7c. The largest value of δ_m is at $m = 0$, so it is expected that cases where δ_0 is smallest have the best agreement between the exact manifold and the Maas−Pope estimate. In ref 1, the attractiveness of the one-dimensional manifolds for the system of this section was characterized by the parameter α_1. For manifolds of type 1, $1/\alpha_1$ is smaller than δ_0 for type 1_1 manifolds and equal to it for type 1_2 manifolds (see ref 1), and therefore the inverse of the attractiveness is an

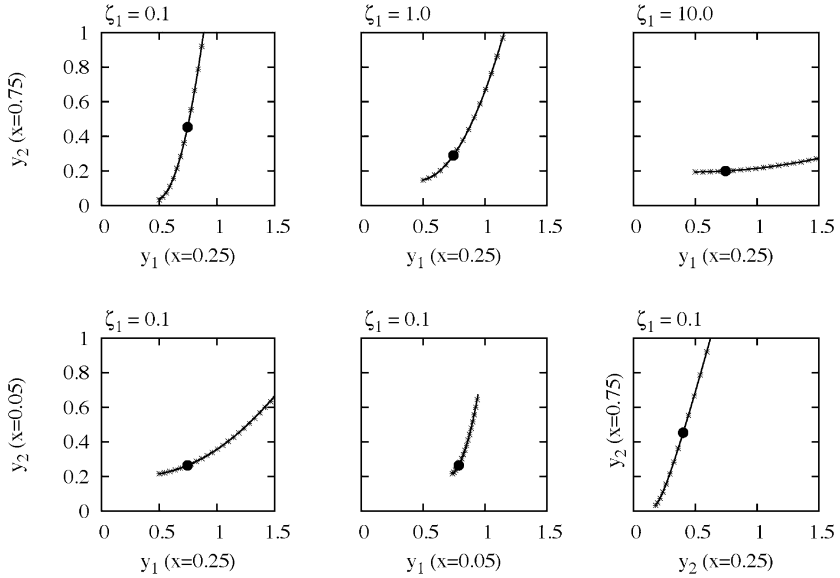

Figure 5. Accuracy of the Maas−Pope estimate of the one-dimensional manifolds. The top row shows a set of plots for three different values of ζ_1 chosen from Figure 10 of ref 1. The triples (ζ_1, ζ_2, ζ_3) (eq 4.11) are from left to right in the top row: (0.1, −0.02, 0.97), (1, −0.85, 0.95), (10.0, −8.6, 0.515). The parameter "*a*" is set to (γ − 2). The bottom row displays the calculation from the top left system at three other projections.

upper bound to δ_0. So it is expected that the Maas−Pope approximation should be reasonably accurate in those regions of parameter space where the manifolds are most attractive (large α). Figure 5 demonstrates that this is true. The three systems were chosen from Figure 10 of ref 1, and all have $\alpha_1 = 8.0$, a fairly high value. These systems have rather small values of δ_0 and so are expected to have good agreement between the exact manifolds and their Maas−Pope estimates. The values of δ_0 are from left to right in the top panels: 0.1, 0.06, and 0.08. The systems are characterized by the following three system parameters[1]

$$\zeta_1 = \frac{D_1 + D_2}{\gamma + 1} \tag{4.11a}$$

$$\zeta_2 = \frac{D_1 - D_2}{\gamma + 1} \quad -\zeta_1 \le \zeta_2 \le \zeta_1 \tag{4.11b}$$

$$\zeta_3 = \frac{\gamma - 1}{\gamma + 1} \quad -1 \le \zeta_3 \le 1 \tag{4.11c}$$

The top row of Figure 5 shows results for three different systems at a specific value of the projection, y_2 ($x = 0.75$) versus y_1 ($x = 0.25$). The bottom row of Figure 5 repeats the calculations of the top left panel at three different projections. The solid lines in Figure 5 show the exact one-dimensional manifolds, and the dots the Maas−Pope estimate of the manifold. These panels indicate that the Maas−Pope algorithm is accurate for highly attractive manifolds.

The Maas−Pope estimate of a manifold is generally less accurate for manifolds whose attractiveness is not high, and this is demonstrated for the one-dimensional manifold in Figure 6 for a system with $\alpha_1 = 4.0$ and $\delta_0 = 0.25$. The solid line shows the exact manifold, the dashed line the Maas−Pope estimate of the manifold, and the dotted lines four different initial distributions. There are larger dots on one of the dotted trajectories to indicate the relative slowness on the manifold. This trajectory and the one emanating from (3.0, 3.5) on the right of the plot clearly are attracted to the exact manifold and miss the Maas−Pope estimate, which is still a fairly accurate representation of the manifold.

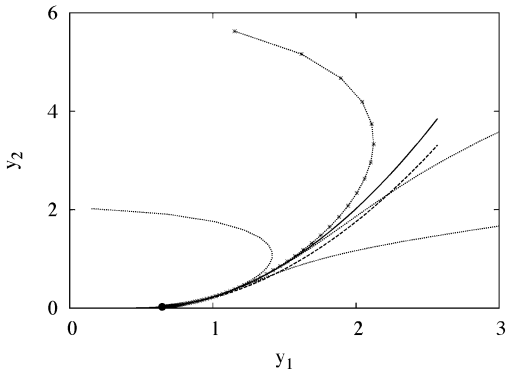

Figure 6. A less attractive one-dimensional manifold than those of Figure 5 shown for (ζ_1, ζ_2, ζ_3) = (0.1, 0.037, 0.84) and $a = 1$. In this case the Maas−Pope estimate (dashed lines) of the manifold (solid line) is somewhat inaccurate. This two-dimensional projection was generated at $y_1(x = 0.8)/y_2(x = 0.2)$.

Figure 7 shows a case where the one-dimensional manifold is not attractive at all, but the two-dimensional manifold is. The top panel shows a y_1/y_2 projection of trajectories, and it is clear that they do not approach a one-dimensional manifold to any significant extent, with the value of α_1 for the one-dimensional manifold being 1.07. However, the value of α_2 for the two-dimensional manifold is 8.24, indicating it is attractive. The bottom panel of Figure 7 demonstrates this attraction, by showing a number of trajectories plotted with solid lines and a two-dimensional manifold plotted as a relatively flat surface with a solid grid. The exact manifold is compared in the bottom panel with the Maas−Pope estimate of the manifold, which clearly is very inaccurate. The inaccuracy can be anticipated because the value of ϵ_0 is 8.24, the same value as α_2. This leads to large errors as calculated with eqs 4.9a and 4.9b. These results are typical of the two-dimensional manifolds labeled as type 1_2 in ref 1.

The results in this section indicate that some care is necessary for calculating one- and two-dimensional manifolds with the Maas−Pope algorithm. Unlike the situation with manifolds for the pure chemical-kinetics situation, the error in the Maas−Pope estimate is not strictly due to the relative attractiveness of the manifolds, nor does it depend on the curvature. Numerical

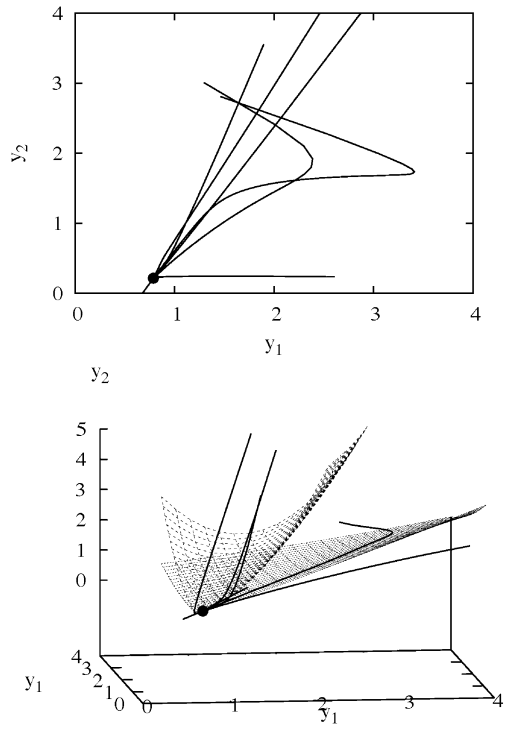

Figure 7. A situation where a one-dimensional manifold is not attractive shown in the top panel. However there is an attractive two-dimensional manifold as shown in the bottom panel. Individual trajectories are plotted as solid lines, and the exact two-dimensional manifold in the bottom panel is drawn with dotted lines and is very attractive ($\alpha_2 = 8.2$). The Maas−Pope estimate of the surface drawn with dashed curves is extremely inaccurate. This inaccuracy can be anticipated from eq 4.9. (ζ_1, ζ_2, ζ_3) = (10, −0.2, 0.33) and $a = 2.0$ for this case. The top panel was generated with a $y_1(x = 0.25)/y_2(x = 0.75)$ projection. The three-dimensional projection in the bottom panel was generated at $y_1(x = 0.25)/y_1(x = 0.60)/y_2(x = 0.37)$.

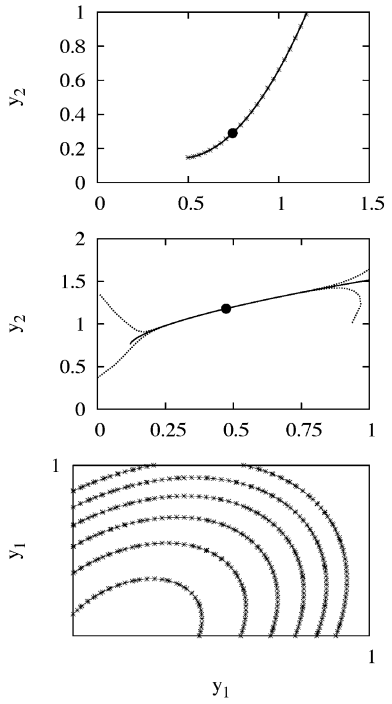

Figure 8. The Maas−Pope estimate vs exact manifold in the top and bottom panel for one-dimensional (top) and two-dimensional manifolds (bottom) for the nonlinear system with an exact manifold. The solid lines show the exact, and the dots show the Maas−Pope estimates. The middle panel compares the Maas−Pope manifold with trajectories for the reaction−diffusion equation for the association reaction (eq 2.5). The top panel is a $y_1(x = 0.25)/y_2(x = 0.75)$ projection, and the middle panel is a $y_1(x = 0.59)/y_2(x = 0.19)$ projection. The bottom panel was generated with a $y_1(x = 0.25)/y_1(x = 0.75)/y_2(x = 0.39)$ projection.

results presented in the rest of the paper show that a Maas−Pope estimate is accurate under many circumstances, but the results in this subsection indicate that some care is necessary when using the algorithm.

B. Manifolds Generated from Numerical Algorithms. The error analysis in the previous subsection, along with Figures 5−7, demonstrated that the Maas−Pope approximation could be accurate but also showed cases where it breaks down. This analysis suggested that the breakdown occurs when the spectra of different rate processes intertwine, making terms such as the ones in eq 4.10 large and thus the error terms in eqs 4.9a and 4.9b large, even though the attractiveness, α_2, is also large. The examples in the rest of the paper avoid this situation. In this subsection, the Maas−Pope algorithm is compared to the more accurate, predictor−corrector method for one-dimensional manifolds, under conditions where it is expected to be accurate, as a way of testing the numerical method for generating the manifolds described in section III. For two-dimensional manifolds, there is no method comparable for high-dimensional systems. Some modifications to the implementation of Fraser's algorithm[5] from ref 14 would be necessary to make that method reasonably efficient for these systems.

The top panel of Figure 8 compares manifolds generated numerically with the analytical Maas−Pope manifolds from the middle top panel of Figure 5. The dots in the top panel show the numerically generated manifold, and the solid line the analytical Maas−Pope approximation. The middle panel of Figure 8 compares the Maas−Pope estimate of the manifold (solid line) with the trajectories of the top panel of Figure 3 (dotted lines). The bottom panel shows a comparison between a two-dimensional manifold generated with the analytical Maas−Pope estimate and the manifold generated numerically. This panel shows the manifold plotted as a set of contours, with the analytical contours plotted with solid lines and the numerically generated contours plotted as series of dots. It is clear from Figure 8 that the numerical algorithm developed in section III generates accurate representations of the Maas−Pope estimates of the manifolds.

Numerically generated Maas−Pope estimates for one-dimensional manifolds are compared to ones estimated with the predictor−corrector algorithm in Figure 9. The top panel of Figure 9 compares the predictor−corrector estimate of the manifold (dots) with the Maas−Pope numerical manifold, which the top panel of Figure 8 demonstrated was accurate. The top panel of Figure 9 thus shows that for a case where the Maas−Pope estimate is accurate the predictor−corrector offers no advantage. However, the middle panel repeats the system of Figure 6. Here the exact manifold is plotted as a solid line, the predictor−corrector as a series of dots, and the Maas−Pope estimate calculated either numerically or from eq 4.5 as a dashed line (they agree). The middle panel of Figure 9 demonstrates that when the Maas−Pope algorithm is inaccurate, the predictor−corrector can be accurate. The bottom panel of Figure 9 compares the Maas−Pope estimate for the manifold (dots) and the predictor−corrector (solid line) for the case of the middle panel of Figure 8. Here again, the predictor−corrector and Maas−Pope estimates agree.

Reference 4 discussed a generic relaxation scenario, as did Appendix A of ref 1, but the results of ref 1 and the present paper show that there is a limit to the attractiveness of manifolds from this scenario. It is also the case that the relaxation pathways

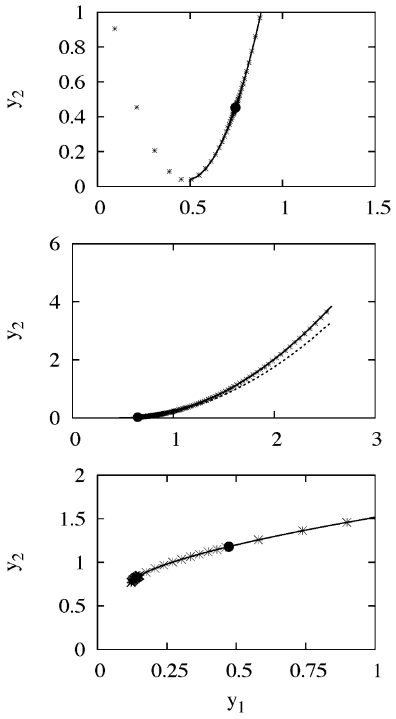

Figure 9. Plots comparing the exact manifold (solid line), predictor−corrector (dots), and Maas−Pope estimates (dotted line in middle panel). The plots demonstrate that the predictor−corrector algorithm makes an accurate estimate of the manifold in the middle panel even when the Maas−Pope estimate is inaccurate. From top to bottom the projections in this figure are: $y_1(x = 0.25)/y_2(x = 0.75)$, $y_1(x = 0.25)/y_2(x = 0.75)$, and $y_1(x = 0.59)/y_2(x = 0.19)$.

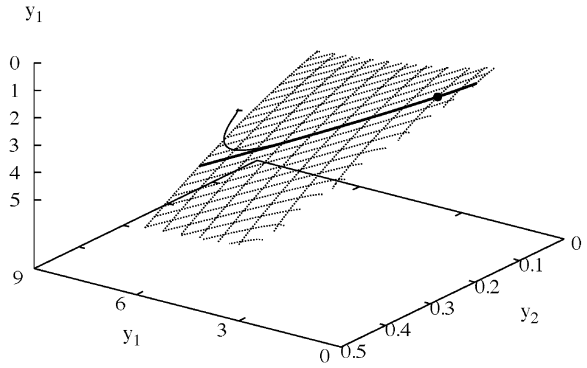

Figure 10. Hierarchy of attractive manifolds for the association reaction case where the two-dimensional manifold is somewhat attractive ($\alpha_2 = 2.6$) and the one-dimensional manifold is more attractive ($\alpha_1 = 8.0$). The projection used in the figure is $y_1(x = 0.6)/y_1(x = 0.3)/y_2(x = 0.2)$.

may be very complicated and difficult to dis-entangle, so a true representation of a hierarchy is difficult to analyze away from equilibrium, where linearization is less informative. However, there are situations where it is possible to observe a hierarchy, and Figure 10 demonstrates this. In Figure 10, the two-dimensional manifold calculated with the Maas−Pope algorithm is plotted as a grid of dotted lines, and the one-dimensional manifold calculated with the algorithm is plotted as a thick solid line. The time propagation of an initial distribution is plotted as a thinner solid line. Figure 10 demonstrates that the distribution first lands on the two-dimensional manifold before it reaches the one-dimensional manifold on the way to equilibrium (large solid dot). The near-equilibrium value of α_1 is 8.0 for the one-dimensional manifold, and α_2 is 2.6 for the two-dimensional manifold. The difference in attractiveness is evident away from equilibrium, because the thin line is much more strongly attracted to the one-dimensional manifold than the two-dimensional manifold.

This subsection and the previous one demonstrate that the numerical procedure to generate a Maas−Pope estimate of the manifold is essentially an exact realization of the analytical version of the same estimate. Although the Maas−Pope estimate of a manifold is generally accurate, the predictor−corrector method is more accurate under conditions where a manifold is not very attractive. No attempt has been made in this paper to generate two-dimensional manifolds in a way that is more accurate than the Maas−Pope algorithm. Because of computational complexity, Fraser's iterative method[5] needs to be modified to make it useful for two-dimensional and higher manifolds. Numerical versions of this algorithm as developed in ref 14 are being considered but have not been developed as yet.

V. Chain-Branching System

This is a system studied earlier by Hadjinicolaou and Goussis[22] and is based on the chain-branching mechanism of Troutman-Dickenson[35]

$$\text{initiation} \quad M_1 \xrightarrow{k_1} R_1 + M_2 \tag{5.1a}$$

$$\text{propagation} \quad R_1 + M_1 \xrightarrow{k_2} R_1H + R_2 \tag{5.1b}$$

$$R_2 \xrightarrow{k_3} R_1 + M_3 \tag{5.1c}$$

$$\text{termination} \quad R_1 + R_2 \xrightarrow{k_4} M_4 \tag{5.1d}$$

The reaction−diffusion equations describing the active species of the system are

$$\frac{\partial R_1}{\partial t} = k_1M_1 - k_2R_1M_1 + k_3R_2 - k_4R_1R_2 + D\frac{\partial^2 R_1}{\partial x^2} \tag{5.2}$$

$$\frac{\partial R_2}{\partial t} = k_2R_1M_1 - k_3R_2 - k_4R_1R_2 + D\frac{\partial^2 R_2}{\partial x^2} \tag{5.2b}$$

$$\frac{\partial M_1}{\partial t} = -k_1M_1 - k_2R_1M_1 + D\frac{\partial^2 M_1}{\partial x^2} \tag{5.2c}$$

This system is a model for an imperfectly stirred reactor, as noted in ref 22. The same variable names are used here for the chemical species, but other designations have been changed. The rate constants are chosen to be the same as one of the numerical examples in ref 22, $k_1 = 1$, $k_2 = 10^3$, and $k_4 = 10^6$, with k_3 varied as it was in ref 22, where the ratio of k_2 and k_3 was singled out as a significant parameter. The boundary conditions are the same as in ref 22, fixed at $x = 0$ ($R_1 = R_2 = 0$, and $M_1 = 1.0$), and no flux at $x = 1.0$ (eq 2.6). The diffusion constants, D, are chosen to be equal in all calculations reported here, but unlike ref 22, they are not always 1.0. Changing D is equivalent to changing the length scale, by making the right boundary different than $x = 1.0$.

It is not clear over what range of the full set of parameters that the system of eq 5.2 possesses strongly attractive one- and two-dimensional manifolds, and only a limited range of parameter space is studied that is consistent with ref 22. Figure 11 shows a set of calculations of the attractiveness of one- and two-dimensional manifolds in the vicinity of the equilibrium.

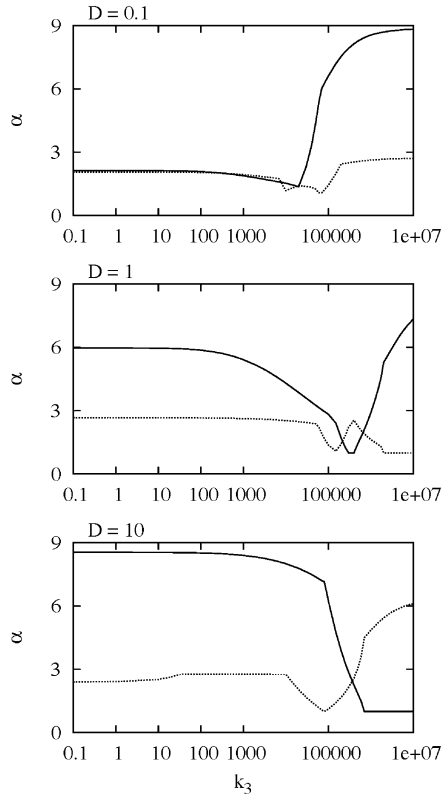

Figure 11. Attractiveness of one-dimensional (solid line) and two-dimensional manifolds (dotted lines) as defined in eqs 2.12 and 2.13 shown for three values of D and a range of values of k_3.

Results for three different diffusion constants are presented over a large range of the rate constant, k_3. The solid lines are values for the one-dimensional manifolds, and the dotted lines are for two-dimensional manifolds. The attractiveness, α, is defined in the usual manner (eqs 2.12 and 2.13). Once again, all eigenvalues have negative real parts, and λ_0 is the eigenvalue that has the lowest magnitude.

Figure 11 demonstrates that while much of parameter space has either attractive one- or two-dimensional manifolds, there are parameter ranges where the attraction is low for small D, which is consistent with ref 1. Several systems with attractive one-dimensional manifolds are studied in Figure 12, which demonstrates that the attractiveness exhibited near equilibrium in Figure 11 extends away from equilibrium. These plots show a one-dimensional manifold as a solid line and a set of results for different initial distributions as dashed lines, which are attracted to the one-dimensional manifolds. The headings list the values of D and k_3. The manifolds were calculated from the Maas−Pope algorithm of section III, and the results indicate that it is very accurate in this case. As noted above, the relaxation can be quite complicated for the systems studied here, because they are infinite-dimensional. The trajectories shown in Figure 12 were generally chosen to be in their last stages of relaxation to the manifold, and this complexity is not always evident in the panels of Figure 12 and other figures in this paper.

The accuracy of the Maas−Pope approximation is confirmed in Figure 13, which compares the Maas−Pope estimates to the more accurate predictor−corrector results. These panels show the predictor−corrector results as solid lines and the Maas−Pope results with a set of dots. The two methods generate manifolds that lie on top of each other.

Figure 11 demonstrated that two-dimensional manifolds are more attractive than one-dimensional manifolds at $D = 10$ for high k_3. Figure 14 shows results for one of these cases, $D = 10$, $k_3 = 5 \times 10^6$. Results for the propagation of five initial distributions are presented in Figure 14, along with the projection of the plane defined by the first two eigenvectors of **J**. This figure demonstrates that there is no attractive one-dimensional manifold ($\alpha_1 = 1.0$), but a fairly attractive two-dimensional manifold is present ($\alpha_2 = 5.9$ near equilibrium).

VI. Ozone System

This section investigates an ozone mechanism studied earlier in refs 17 and 25. The same rate parameters are used as in these earlier papers, but simulations are run under isothermal conditions. There are three species: O, O_2, and O_3. As in the earlier references, it is assumed that diffusivity is spatially constant. In the present study several different sets of equal diffusion constants are investigated, with the spatial domain set to 1.0. Some results are presented for unequal diffusion constants, as was done in Figure 1 of the first paper[1]. The system in that figure had different fixed boundary conditions at $x = 0$, that are set to the following here: [O] ($x = 0$) = 0.0, [O_2] ($x = 0$) = 2×10^{-5} mol/cm^3, [O_3]($x = 0$) = 1×10^{-5} mol/cm^3.

The reaction−diffusion system under these conditions is

$$\frac{\partial[\mathrm{O}]}{\partial t} = F_{\mathrm{O}} + D_1 \frac{\partial^2[\mathrm{O}]}{\partial x^2} \tag{6.1a}$$

$$\frac{\partial[\mathrm{O_2}]}{\partial t} = F_{\mathrm{O_2}} + D_2 \frac{\partial^2[\mathrm{O_2}]}{\partial x^2} \tag{6.1b}$$

$$\frac{\partial[\mathrm{O_3}]}{\partial t} = F_{\mathrm{O_3}} + D_3 \frac{\partial^2[\mathrm{O_3}]}{\partial x^2} \tag{6.1c}$$

The F values are described by the same mass-action kinetics used throughout this paper and are presented more completely in refs 17 and 25.

The attractiveness of one- and two-dimensional manifolds near equilibrium is presented in Figure 15 as a function of temperature at several different values of D and for one case where the D values are different (bottom). Over most of the temperature range there are attractive one- and two-dimensional manifolds. This case is like the reversible association reaction of section II, because the chemical kinetics possesses a constant of motion due to conservation of the elements

$$[\mathrm{O}] + 2[\mathrm{O_2}] + 3[\mathrm{O_3}] = c \tag{6.2}$$

Results for a select set of temperatures and D values are presented in Figure 16. Figure 16a shows results for $T = 880$ K and $D = 100$, Figure 16b has results for $T = 1200$ and $D = 100$, and Figure 16c presents results for $D = 1000$ and $T = 1100$ K. These plots are two-dimensional projections, which are described in the figure caption. The attractiveness of the manifolds can be read off Figure 15 and are from top to bottom: (a) $\alpha_1 = 9.0$, (b) $\alpha_1 = 9.0$, and (c) $\alpha_1 = 5.0$. Results for four different distributions are shown in each panel of Figure 16 as dashed lines, and an estimate of the one-dimensional manifolds using the Maas−Pope algorithm is plotted as thicker solid lines. Figure 16 demonstrates that trajectories are attracted strongly to the manifold and that the Maas−Pope estimate of the manifold is accurate.

As indicated in Figure 15, there are temperature ranges where two-dimensional manifolds are more attractive than one-dimensional manifolds near equilibrium. Figure 17 shows results for one of these cases. The temperature is 600 K and $D = 1000$.

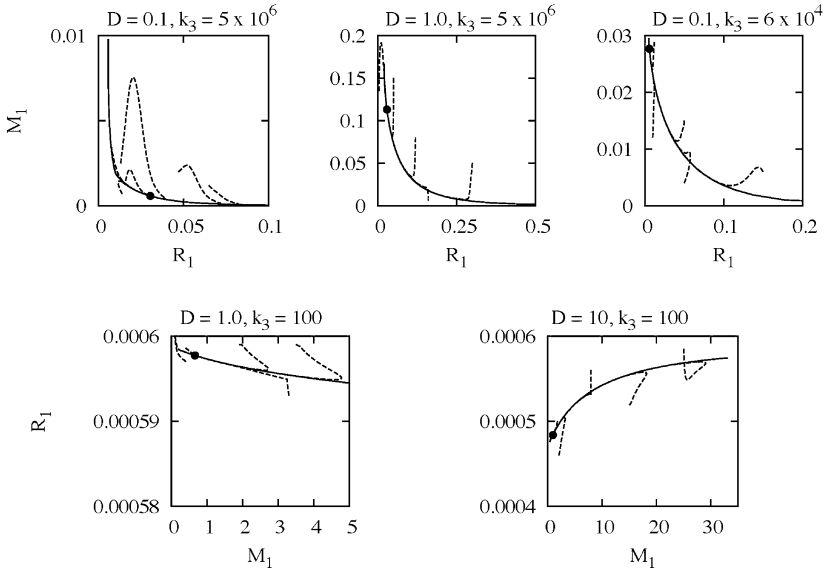

Figure 12. Trajectories (dashed lines) are presented for five sets of systems as they approach a one-dimensional manifold. The systems are from Figure 11, and the manifolds were estimated with the Maas−Pope algorithm. The projections are listed in the axes labels, and the headings show the values of D and k_3, with all other parameters described in the text. The top row shows $R_1(x = 0.54)/M_1(x = 0.44)$ projections, and the bottom row shows $M_1(x = 0.44)/R_1(x = 0.08)$ projections.

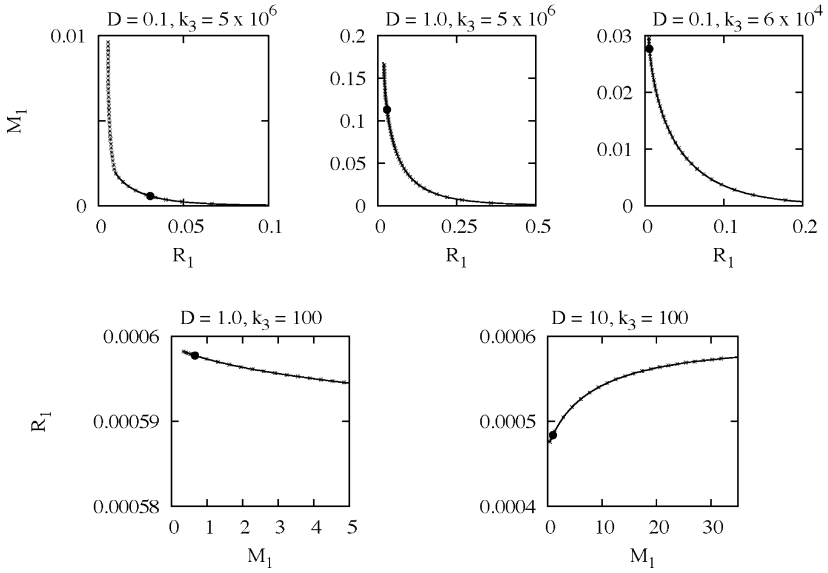

Figure 13. Results for the same set of manifolds as Figure 12 shown here, comparing the Maas−Pope estimate (dots) with the predictor−corrector (solid lines) estimate. Each of the panels has the same projections as those in Figure 12.

The attractiveness of the two-dimensional manifold is $\alpha_2 = 8.98$. In this figure results are shown for six distributions as solid lines, and an estimate of the two-dimensional manifold calculated with the Maas−Pope algorithm is shown as a dotted-line grid. Because the attractiveness of the one-dimensional manifold is so weak ($\alpha_1 = 1.001$) there is no apparent attraction to it. But it is clear from Figure 17 that the two-dimensional manifold is attractive away from equilibrium.

The Maas−Pope algorithm is a convenient method to generate manifolds, and we compare it to the more accurate but more time-consuming predictor−corrector method. In Figure 18, the three manifolds from Figure 16 are once again plotted, this time as a series of dots. The predictor−corrector values of the manifolds are plotted as solid lines in Figure 18. It is clear that there is good agreement between the predictor−corrector estimate and the Maas−Pope estimate, although there is some small but noticeable disagreement at the smallest values of the O_2 concentration in the top two panels. The results in this figure demonstrate that while it is possible to find situations (for example, Figure 6) where the Maas−Pope algorithm is inaccurate, it is an accurate estimate for most situations where the manifold is very attractive.

VII. Conclusion

This paper has numerically investigated the nature of one- and two-dimensional manifolds of several reaction−diffusion systems as they approach equilibrium. This extends the analysis of the first paper[1] to more realistic systems and systems that are amenable to only numerical analysis.

To extend the analysis, it was necessary to adapt two methods for finding low-dimensional manifolds to the reaction−diffusion cases studied here. The predictor−corrector method of ref 14 required little change, but the Maas−Pope algorithm of refs 9−11 required modifications. Because the reaction−diffusion systems have infinite spectra, necessarily truncated numerically,

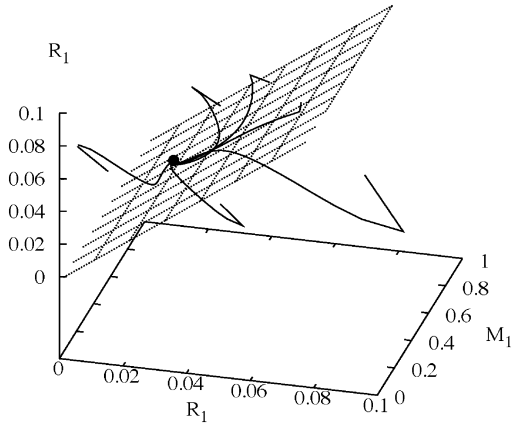

Figure 14. Plot showing a case where a two-dimensional manifold is attractive, but there is no attractive one-dimensional manifold. The parameters are $D = 10$ and $k_3 = 5 \times 10^6$. The values of $\alpha_1 = 1.0$ and $\alpha_2 = 5.9$ (eqs 2.12 and 2.13). The projection shown in this plot is $R_1(x = 0.54)/M_1(x = 0.44)/R_1(x = 0.90)$.

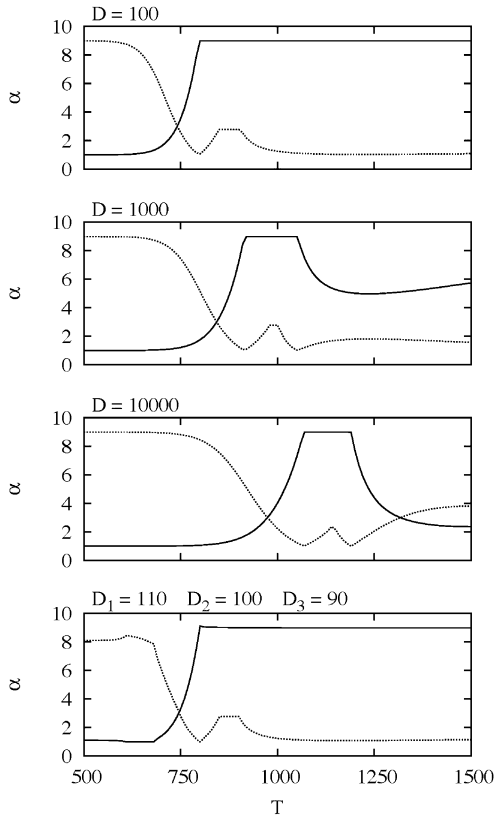

Figure 15. Attractiveness for the ozone example near equilibrium is shown for one-dimensional (solid lines) and two-dimensional (dotted lines) manifolds plotted vs temperature for several different values of *D*. The top three panels have equal *D* values, and the bottom panel shows unequal *D* values.

it became important to have an algorithm that only used the relevant eigenvectors, the so-called slow space. Once this was done it was straightforward to develop an algorithm that was faster, because it used eigenvector derivatives that required much less computation. The modified algorithm ran faster by a factor of approximately 50 for the problems studied here.

The reduction achieved with the low-dimensional manifolds studied here is orders of magnitude greater than the reduction from methods that reduce the number of species, because both the number of species and the number of grid points are reduced. For example, in many of the problems studied here the one-dimensional manifold represents a reduction from 300 ordinary differential equations to one.

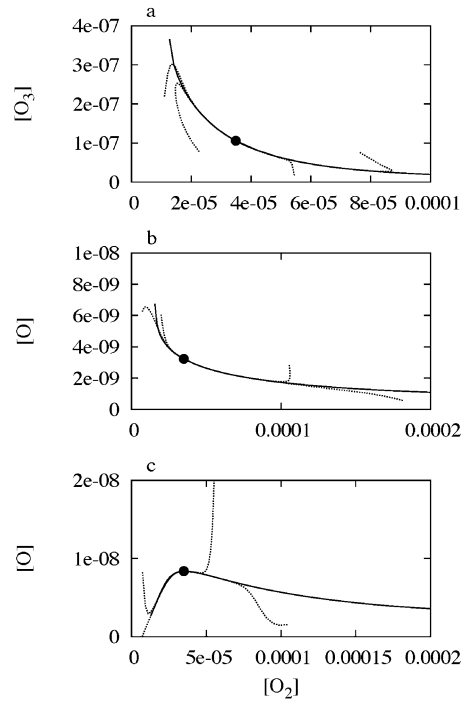

Figure 16. Plots showing how trajectories are attracted to one-dimensional manifolds for the ozone system. The dotted lines show trajectories, and the solid lines show manifolds estimated with the Maas−Pope algorithm. The *D* values and *T* values vary for each plot, but the *D* values are equal for each case. The values of *D* and *T* are: (a) $D = 100$, $T = 880$ K, (b) $D = 100$, $T = 1200$ K, and (c) $D = 1000$, $T = 1100$ K. Concentrations are in mol/cm^3. The projections for the top two panels are $y_1(x = 0.46)/y_2(x = 0.46)$, and for the bottom panel $y_1(x = 0.46)/y_2(x = 0.68)$.

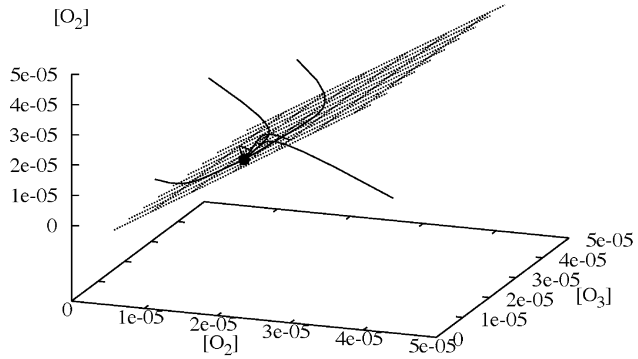

Figure 17. At $D = 10\,000$ and $T = 600$ K the one-dimensional manifold is not particularly attractive (Figure 16) ($\alpha_1 = 1.0001$), and the two-dimensional manifold is ($\alpha_2 = 8.995$), as demonstrated in the figure. The projections shown in this figure are $y_1(x = 0.46)/y_1(x = 0.68)/y_2(x = 0.46)$.

Although the reductions outlined here are significant, they occur at the longest times. This means that there are many physical and chemical processes where they are not useful, because these processes occur at shorter times. The reduction techniques studied here could be used for more general physical processes if they were defined locally in space. Attention to this problem is underway.

Acknowledgment. This work was supported by the Office of Basic Energy Sciences, Division of Chemical Sciences, Geosciences, and Biosciences, U. S. Department of Energy, under Contract No. W-31-109-ENG-38.

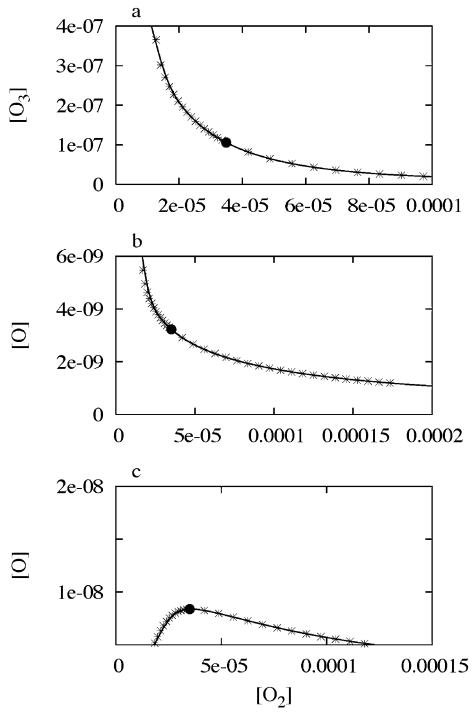

Figure 18. Plots comparing the manifolds from Figure 17 (dots here) generated by the Maas−Pope estimate with predictor−corrector results (solid lines). The projections are the same for each panel as they are in Figure 16.

Appendix A: Exact Realization of Maas−Pope Approximation for a Nonlinear Reaction−Diffusion System

For the system of eq 4.1 it is possible to analytically generate the Maas−Pope approximation to the exact manifolds presented in ref 1. The distributions for y_1 and y_2 are expanded in terms of the eigenvectors of the diffusion equation

$$y_1(x,t) = y_1^{\mathrm{eq}}(x) + \sum_m b_{1m}(t) \sin\left[\left(m+\frac{1}{2}\right)\pi x\right] \quad \text{(A.1a)}$$

and

$$y_2(x,t) = y_2^{\mathrm{eq}}(x) + \sum_m b_{2m}(t) \sin\left[\left(m+\frac{1}{2}\right)\pi x\right] \quad \text{(A.1b)}$$

These expansions are inserted into eq 4.1 giving

$$\frac{\mathrm{d}b_{1m}}{\mathrm{d}t} = -\left[1+\left(m+\frac{1}{2}\right)^2\pi^2 D_1\right] b_{1m} \quad \text{(A.2a)}$$

$$\frac{\mathrm{d}b_{2m}}{\mathrm{d}t} = -\left[\gamma+\left(m+\frac{1}{2}\right)^2\pi^2 D_2\right] b_{2m} + 2a\sum_j S_j^m b_{1j} + a\sum_k\sum_n r_{kn}^m b_{1k} b_{1n} \quad \text{(A.2b)}$$

$$r_{kn}^m = 2\int \sin\left[\left(m+\frac{1}{2}\right)\pi x\right] \sin\left[\left(k+\frac{1}{2}\right)\pi x\right] \sin\left[\left(n+\frac{1}{2}\right)\pi x\right] \mathrm{d}x \quad \text{(A.3a)}$$

$$s_j^m = 2\int y_1^{\mathrm{eq}} \sin\left[\left(m+\frac{1}{2}\right)\pi x\right] \sin\left[\left(j+\frac{1}{2}\pi x\right)\right] \mathrm{d}x \quad \text{(A.3b)}$$

The Jacobian matrix of the system in eq A.2 is written in the following form The blocks have the following matrix elements

$$\mathbf{J} = \begin{pmatrix} J^{11} & J^{12} \\ J^{21} & J^{22} \end{pmatrix} \quad \text{(A.4)}$$

$$J_{km}^{11} = 0 \quad \text{except} \quad J_{kk}^{11} = -\left[1+\left(k+\frac{1}{2}\right)^2\pi^2 D_1\right] \quad \text{(A.5a)}$$

$$J_{km}^{21} = 2aS_m^k + 2a\sum_n r_{mn}^k b_{1n} \quad \text{(A.5b)}$$

$$J_{km}^{12} = 0 \quad \text{(A.5c)}$$

$$J_{km}^{22} = 0 \quad \text{except} \quad J_{kk}^{22} = -\left[\gamma+\left(k+\frac{1}{2}\right)^2\pi^2 D_2\right] \quad \text{(A.5d)}$$

There are two sets of eigenvalues

$$\lambda_k^1 = -\left[1+\left(k+\frac{1}{2}\right)^2\pi^2 D_1\right] \quad \text{(A.6a)}$$

$$\lambda_k^2 = -\left[\gamma+\left(k+\frac{1}{2}\right)^2\pi^2 D_2\right] \quad \text{(A.6b)}$$

For one-dimensional manifolds of type 1 (ref 1) the lowest eigenvalue is λ_0^1. The right eigenvectors are written as

$$\mathbf{R} = \begin{pmatrix} R^{11} & R^{12} \\ R^{21} & R^{22} \end{pmatrix} \quad \text{(A.7)}$$

It is straightforward to find the eigenvectors. For the algorithm outlined in section III, the following eigenvector is needed for one-dimensional manifolds of type 1

$$R_{m0}^{11} = 0 \quad \text{except} \quad R_{00}^{11} = 1 \quad \text{(A.8a)}$$

$$R_{m0}^{21} = \frac{2aS_m^0 + 2a\sum_n r_{mn}^0 b_{1n}}{(\gamma-1)+\left(m+\frac{1}{2}\right)^2\pi^2 D_2 - \frac{\pi^2 D_1}{4}} \quad \text{(A.8b)}$$

The idea behind the Maas−Pope algorithm[9] is that a one-dimensional attractive manifold is such that the velocity vector of the system (the right-hand side of eq A.2) lines up along this eigenvector. The calculation of the conditions that need to be satisfied are first described for the R^{11} components of the eigenvector

$$\frac{R_{m0}^{11}}{R_{00}^{11}} = \frac{-\left[1+\left(m+\frac{1}{2}\right)^2\pi^2 D_1\right] b_{1m}}{-\left[1+\frac{\pi^2 D_1}{4}\right] b_{10}} \quad \text{(A.9)}$$

Equation A.9 is merely a statement that the velocity vector component (right-hand ratio) lines up along the proper eigenvector component (left-hand ratio). The values of R^{11} can be substituted from eq A.8a

$$0 = \frac{-\left[1+\left(m+\frac{1}{2}\right)^2\pi^2 D_1\right]b_{1m}}{-\left[1+\frac{\pi^2 D_1}{4}\right]b_{10}} \Rightarrow b_{1\mathrm{m}} = 0 \quad m \neq 0 \tag{A.10}$$

This indicates that all of the b_{1m} values are zero except b_{10}.

The results for the b_{1m} values can be used to solve for the b_{2m} values employing the correct components of R^{21} and the corresponding velocity components

$$\frac{R^{21}_{m0}}{R^{11}_{00}} = \frac{-\left[\gamma+\left(m+\frac{1}{2}\right)^2\pi^2 D_2\right]b_{2m} + 2aS_0^m b_{10} + ar_{00}^m b_{10}^2}{-\left[1+\frac{\pi^2 D_1}{4}\right]b_{10}} \tag{A.11a}$$

$$b_{2m} = \frac{\left[1+\frac{\pi^2 D_1}{4}\right]b_{10}R^{21}_{m0} + 2aS_0^m b_{10} + ar_{00}^m b_{10}^2}{\left[\gamma+\left(m+\frac{1}{2}\right)^2\pi^2 D_2\right]} \tag{A.11b}$$

The velocity components defined on the right-hand side of eq A.2b are simplified because all of the b_1 values are zero except b_{10}. The R^{21} components in eq A.11b are defined in eq A.8b, with the summation truncated to a single term, because only b_{10} is nonzero. The b_{2m} values are now

$$b_{2m} = \alpha_m b_{10} + \beta_m b_{10}^2 \tag{A.12}$$

with

$$\alpha_m = \frac{2aS_0^m}{\left[(\gamma-1)+\left(m+\frac{1}{2}\right)^2\pi^2 D_2 - \frac{\pi^2 D_1}{4}\right]} \tag{A.13a}$$

and

$$\beta_{\mathrm{m}} = \frac{\mathrm{a}\left[(\gamma+1)+\left(\mathrm{m}+\frac{1}{2}\right)^2\pi^2\mathrm{D}_2+\frac{\pi^2\mathrm{D}_1}{4}\right]\mathrm{r}_{00}^{\mathrm{m}}}{\left[(\gamma-1)+\left(\mathrm{m}+\frac{1}{2}\right)^2\pi^2\mathrm{D}_2-\frac{\pi^2\mathrm{D}_1}{4}\right]\left[\gamma+\left(\mathrm{m}+\frac{1}{2}\right)^2\pi^2\mathrm{D}_2\right]} \tag{A.13b}$$

The Maas−Pope approximation for two-dimensional manifolds of type 1_1 is defined in the following manner. The velocity vector is lined up in the plane of the first two right eigenvectors

$$f_{01}\frac{\mathrm{d}b_{qm}}{\mathrm{d}t} - f_{1m}\frac{\mathrm{d}b_{10}}{\mathrm{d}t} - f_{0m}\frac{\mathrm{d}b_{11}}{\mathrm{d}t} = 0 \quad q = 1, 2 \tag{A.14a}$$

$$f_{01} = R^{11}_{00}R^{11}_{11} - R^{11}_{10}R^{11}_{01} \tag{A.14b}$$

$$f_{0m} = R^{11}_{00}R_{m1} - R_{m0}R^{11}_{01} \tag{A.14c}$$

$$f_{1m} = R^{11}_{11}R_{m0} - R^{11}_{10}R_{m1} \tag{A.14d}$$

Note that it is assumed that the "progress variables" are b_{10} and b_{11}. Equation A.14a is rewritten substituting the velocities from eq A.2

$$-(R^{11}_{00}R^{11}_{11} - R^{11}_{10}R^{11}_{01})\left[1+\left(m+\frac{1}{2}\right)^2\pi^2 D_1\right]b_{1m} + \left(1+\frac{\pi^2 D_1}{4}\right)f_{1m}b_{10} + f_{0m}\left(1+\frac{9\pi^2 D_1}{4}\right)b_{11} = 0 \quad q = 1, 2 \tag{A.15}$$

Equation A.15 can be used to solve for b_{1m}

$$-(R^{11}_{00}R^{11}_{11} - R^{11}_{10}R^{11}_{01})\left[1+\left(m+\frac{1}{2}\right)^2\pi^2 D_1\right]b_{1m} = 0 \Rightarrow b_{1m} = 0 \quad m \neq 0, 1 \tag{A.16}$$

The solution for b_{1m} yields the following solution for b_{2m}

$$(R^{11}_{00}R^{11}_{11} - R^{11}_{10}R^{11}_{01})\frac{\mathrm{d}b_{2m}}{\mathrm{d}t} + \left(1+\frac{\pi^2 D_1}{4}\right)f_{1m}b_{10} + f_{0m}\left(1+\frac{9\pi^2 D_1}{4}\right)b_{11} = 0 \tag{A.17a}$$

$$\frac{\mathrm{d}b_{2m}}{\mathrm{d}t} = \frac{-\left[\left(1+\frac{\pi^2 D_1}{4}\right)f_{1m}b_{10} + f_{0m}\left(1+\frac{9\pi^2 D_1}{4}\right)b_{11}\right]}{(R^{11}_{00}R^{11}_{11} - R^{11}_{10}R^{11}_{01})} \tag{A.17b}$$

Through the use of eq A.2a and the solution for b_{1m} in eq A.16, the b_{2m} velocities can also be written as

$$\frac{\mathrm{d}b_{2m}}{\mathrm{d}t} = -\left[\gamma+\left(m+\frac{1}{2}\right)^2\pi^2 D_2\right]b_{2m} + 2a(b_{10}S_0^m + b_{11}S_1^m) + a(r_{00}^m b_{10}^2 + 2r_{10}^m b_{10}b_{11} + r_{11}^m b_{11}^2) \tag{A.18}$$

Equations A.17b and A.18 can be used to solve for b_{2m}, which is written as

$$b_{2m} = \eta_{0m}b_{10} + \eta_{1m}b_{11} + \tau_{1m}b_{10}^2 + \tau_{2m}b_{10}b_{11} + \tau_{3m}b_{11}^2 \tag{A.19}$$

using these relationships

$$f_{0m} = R^{21}_{m1} \tag{A.20a}$$

$$f_{1m} = R^{21}_{m0} \tag{A.20b}$$

$$R^{21}_{m0} = \frac{2aS_0^m + 2a(r_{00}^m b_{10} + r_{01}^m b_{11})}{(\gamma-1)+\left(m+\frac{1}{2}\right)^2\pi^2 D_2 - \frac{\pi^2 D_1}{4}} \tag{A.20c}$$

$$R^{21}_{m1} = \frac{2aS_1^m + 2a(r_{01}^m b_{10} + r_{11}^m b_{11})}{(\gamma-1)+\left(m+\frac{1}{2}\right)^2\pi^2 D_2 - \frac{9\pi^2 D_1}{4}} \tag{A.20d}$$

The coefficients in eq A.19 have the following form

$$\eta_{0m} = \frac{2aS_0^m}{\left[(\gamma-1)+\left(m+\frac{1}{2}\right)^2\pi^2 D_2 - \frac{\pi^2 D_1}{4}\right]} \tag{A.21a}$$

$$\eta_{1m} = \frac{2aS_1^m}{\left[(\gamma - 1) + \left(m + \frac{1}{2}\right)^2 \pi^2 D_2 - \frac{9\pi^2 D_1}{4}\right]} \quad \text{(A.21b)}$$

$$\tau_{1m} = \frac{\left[(\gamma + 1) + \left(m + \frac{1}{2}\right)^2 \pi^2 D_2\right] + \frac{\pi^2 D_1}{4} a r_{00}^m}{\left[(\gamma - 1) + \left(m + \frac{1}{2}\right)^2 \pi^2 D_2 - \frac{\pi^2 D_1}{4}\right]\left[\gamma + \left(m + \frac{1}{2}\right)^2 \pi^2 D_2\right]} \quad \text{(A.21c)}$$

$$\tau_{2m} = \frac{2a\left\{\left[\gamma + \left(m + \frac{1}{2}\right)^2 \pi^2 D_2\right]^2 - \left(1 + \frac{\pi^2 D_1}{4}\right)\left(1 + \frac{9\pi^2 D_1}{4}\right)\right\} r_{01}^m}{\left[(\gamma - 1) + \left(m + \frac{1}{2}\right)^2 \pi^2 D_2 - \frac{9\pi^2 D_1}{4}\right]\left[(\gamma - 1) + \left(m + \frac{1}{2}\right)^2 \pi^2 D_2 - \frac{\pi^2 D_1}{4}\right]\left[\gamma + \left(m + \frac{1}{2}\right)^2 \pi^2 D_2\right]} \quad \text{(A.21d)}$$

$$\tau_{3m} = \frac{\left[(\gamma + 1) + \left(m + \frac{1}{2}\right)^2 \pi^2 D_2 + \frac{9\pi^2 D_1}{4}\right] a r_{11}^m}{\left[(\gamma - 1) + \left(m + \frac{1}{2}\right)^2 \pi^2 D_2 - \frac{9\pi^2 D_1}{4}\right]\left[\gamma + \left(m + \frac{1}{2}\right)^2 \pi^2 D_2\right]} \quad \text{(A.21e)}$$

References and Notes

(1) Davis M. J. *J. Phys. Chem A* **2006**, *110*, 5235.

(2) For example, see: (a) Oran E. S.; Boris, J. P. *Numerical Simulation of Reactive Flows*; Cambridge University Press: Cambridge, U. K., 2001. (b) Warnatz, J.; Maas, U.; Dibble, R. W. *Combustion*; Springer: New York, 2001. (c) Kee, R. J.; Coltrin, M. E.; Glarborg, P. *Chemical Reacting Flow: Theory and Practice*; Wiley-Interscience: New York, 2003.

(3) (a) Griffiths, J. F. *Prog. Energy Combust. Sci.* **1995**, *21*, 25. (b) Tomlin, A. S.; Turányi, T.; and Pilling, M. J. in *Low-Temperature Combustion and Autoignition*; Pilling, M. J., Ed.; Comprehensive Chemical Kinetics 35; Elsevier: New York, 1997; p 293. (c) Okino M. S.; Mavrovouniotis, M. L. *Chem. Rev.* **1998**, *98*, 243.

(4) Roussel, M. R. A Rigorous Approach to Steady-State Kinetics Applied to Simple Enzyme Mechanisms. Ph.D. Thesis, University of Toronto, 1994.

(5) Fraser, S. J. *J. Chem. Phys.* **1988**, *88*, 4732.

(6) (a) Roussel M. R.; Fraser, S. J. *J. Chem. Phys.* **1990**, *93*, 1072. (b) Roussel M. R.; Fraser, S. J. *J. Chem. Phys.* **1991**, *94*, 7106. (c) Roussel M. R.; Fraser, S. J. *J. Phys. Chem.* **1991**, *95*, 8762. (d) Roussel, M. R.; Fraser, S. J. *J. Phys. Chem.* **1993**, *97*, 8316. (e) Roussel, M. R.; Fraser, S. J. *J. Phys. Chem.* **1994**, *98*, 5174. (f) Fraser S. J.; Roussel, M. R. *Can. J. Chem.* **1994**, *72*, 800. (g) Fraser, S. J. *J. Chem. Phys.* **1998**, *109*, 411.

(7) (a) Nguyen, A. H.; Fraser, S. J. *J. Chem. Phys.* **1989**, *91*, 186. (b) Roussel, M. R. *J. Math. Chem.* **1997**, *21*, 385. (c) Roussel, M. R.; Fraser, S. J. *Chaos* **2001**, *11*, 196.

(8) Lam S. H.; Goussis, D. A. *Int. J. Chem. Kinet.* **1994**, *26*, 461. For recent developments and important applications, for example, see: Valorani, M.; Najm, H. N.; Goussis, D. A. *Combust. Flame* **2003**, *134*, 35 and references cited there.

(9) (a) Maas, U.; Pope, S. B. *Combust. Flame* **1992**, *88*, 239. (b) Maas, U.; Pope, S. B. *Proc. Combust. Inst.* **1992**, *28*, 103.

(10) Maas, U.; Pope, S. B. *Proc. Combust. Inst.* **1994**, *25*, 1349.

(11) Maas, U. *Comput. Visualization Sci.* **1998**, *1*, 69.

(12) Recent applications and algorithm developments concerning the Maas−Pope algorithm by Maas and co-workers can be found in: (a) Maas, U. *Appl. Math.* **1995**, *3*, 249. (b) Schmidt, D.; Maas, U.; Segatz, J.; Reidel, U.; Warnatz, J. *Combust. Sci. Technol.* **1996**, *113*, 3. (c) Deuflhard, P.; Heroth, J.; Maas, U. In *Modeling of Chemical Reaction Systems, Proceedings of an International Workshop (Heidelberg)*; Warnatz J., Behrendt, F., Eds.; Springer: Berlin, 1996. (d) Neimann, H.; Schmidt, D.; Maas, U. *J. Eng. Math.* **1997**, *31*, 131. (e) Schmidt, D.; Blasenberg, T.; Maas, U. *Combust. Theory Modeling* **1998**, *2*, 135. (f) Yan, X.; Maas, U. *Proc. Combust. Inst.* **2000**, *28*, 1615.

(13) Other recent applications and algorithm developments of the Maas−Pope algorithm can be found, for example, in: (a) Eggels, R. L. G. M.; de Goey, L. P. H. *Combust. Flame* **1995**, *100*, 559. (b) Eggels, R. L. G. M.; de Goey, L. P. H. *Combust. Sci. Technol.* **1995**, *107*, 165. (c) Deuflhard P.; Heroth, J. In *Scientific Computing in Chemical Engineering*; Keil, F., Mackens, W., Voss, H., Werther, J., Eds.; Springer: Berlin, 1996; p 29. (d) Eggels, R. L. G. M.; Louis, J. J. B.; Kok, B. W.; de Goey, L. P. H. *Combust. Sci. Technol.* **1997**, *123*, 347. (e) Gicquel, O.; Thevenin, D.; Hilka, M.; Darabiha, N. *Combust. Theory Model.* **1999**, *3*, 479. (f) Rhodes, C.; Morari, M.; Wiggins, S. *Chaos* **1999**, *9*, 108. (g) Singh, S.; Rastigejev, Y.; Paolucci, S.; Powers, J. M. *Combust. Theory Model.* **2001**, *5*, 163.

(14) Davis, M. J.; Skodje, R. T. *J. Chem. Phys.* **1999**, *111*, 859.

(15) Skodje, R. T.; Davis, M. J. *J. Phys. Chem. A* **2001**, *105*, 10356.

(16) Davis, M. J.; Skodje, R. T. *Z. Phys. Chem.* **2001**, *215*, 233.

(17) Singh, S.; Powers, J. M.; Paolucci, S. *J. Chem. Phys.* **2002**, *117*, 1482.

(18) Lowe, R.; Tomlin, A. *Atmos. Environ.* **2000**, *34*, 2425.

(19) Schwer, Schwer; Lu, P.; Green, W. H.; Semiao, V. *Combust. Theory Model.* **2003**, *7*, 383.

(20) Lebiedz, D. *J. Chem. Phys.* **2004**, *120*, 6890.

(21) Yannacopoulos, A. N.; Tomlin, A. S.; Brindley, J.; Merkin, J. H.; Pilling, M. J. *Physica D* **1994**, *83*, 421.

(22) Hadjinicolaou, M.; Goussis, D. A. *SIAM J. Sci. Comput.* **1999**, *20*, 781.

(23) Robinson, J. C. *Chaos* **1995**, *5*, 330.

(24) (a) Temam, R. *Infinite-Dimensional Dynamical Systems in Mechanics and Physics*; Applied Mathematical Sciences 68; Springer-Verlag: New York, 1988. (b) Robinson, J. C. *Infinite-Dimensional Dynamical Systems: An Introduction to Dissipative Parabolic PDEs and the Theory of Global Attractors*; Cambridge University Press: Cambridge, U. K., 2001.

(25) Margolis, S. B. *J. Comput. Phys.* **1978**, *27*, 410.

(26) For a good discussion of the solution of the equilibrium problem, for example, see: Kee, R. J.; Grcar, J. F.; Smooke, M. D.; Miller, J. A. *A Fortran Program for Modeling Steady Laminar One-Dimensional Premixed Flames*; SAND85-8240; Sandia National Laboratories: Albuquerque, NM, 1985.

(27) There are discussions of this technique in many places, for example, see ref 2.

(28) Logan, J. D. *Applied Partial Differential Equations*, 2nd ed., Springer: New York, 2004. Chapter 5.3 has a discussion of the stability analysis of partial differential equations.

(29) Hundsdorfer W.; Verwer, J. G. *Numerical Solution of Time-Dependent Advection−Diffusion−Reaction Equations*; Springer: Berlin, 2003.

(30) Hindmarsh, A. C. In *Scientific Computing*; Stepleman, R. S. et al., Eds.: North-Holland: Amsterdam, 1983; p 55.

(31) Golub G. H.; Van Loan, C. F. *Matrix Computations*; Johns Hopkins University Press: Baltimore, MD, 1996.

(32) For example, see: Press, W. H.; Teukolsky, S. A.; Vetterling, W. T.; Flannery, B. P. *Numerical Recipes*; Cambridge University Press: Cambridge, U. K., 1992.

(33) Nelson, R. B. *AIAA J.* **1976**, *14*, 1201.

(34) Kaper. H. J.; Kaper, T. J. *Physica D* **2002**, *165*, 66.

(35) Troutman-Dickenson, A. F. *Gas Kinetics*; Butterworth: London, 1955.